RESEARCH ARTICLE

Key Points:
- We provide $^{40}Ar/^{39}Ar$ age determinations for Tahitian lava flows bracketing the Matuyama-Bruhnes reversal
- A ~33 kyr period of magnetic field instability preceded the final reversal
- A stochastic model is presented that reconciles age constraints between lava flow and sediment archives

Millennial-Scale Instability in the Geomagnetic Field Prior to the Matuyama-Brunhes Reversal

Andrea Marie Balbas[1,2] , Anthony A. P. Koppers[1] , Peter U. Clark[1], Robert S. Coe[3] , Brendan T. Reilly[1] , Joseph S. Stoner[1], and Kevin Konrad[1]

[1]College of Earth, Ocean and Atmospheric Sciences, Oregon State University, Corvallis, OR, USA, [2]Divison of Geological and Planetary Sciences, California Institute of Technology, Pasadena, CA, USA, [3]Earth and Planetary Science Department, University of California–Santa Cruz, Santa Cruz, CA, USA

Abstract Changes in the Earth's magnetic field have global significance that reach from the outer core extending out to the uppermost atmosphere. Paleomagnetic records derived from sedimentary and volcanic sequences provide important insights into the geodynamo processes that govern the largest geomagnetic changes (polarity reversals), but dating uncertainties have hindered progress in this understanding. Here, we report a paleomagnetic record from multiple lava flows on Tahiti that bracket the Matuyama-Brunhes (M-B) polarity reversal ~771,000 years ago. Our high-precision $^{40}Ar/^{39}Ar$ ages constrain several rapid and short-lived changes in field orientation up to 33,000 years prior to the M-B reversal. These changes are similar to ones identified in other less well-dated lava flows in Maui, Chile, and La Palma that occurred during an extended period of reduced field strength recorded in sediments. We use a simple stochastic model to show that these rapid polarity changes are highly attenuated in sediment records with low sedimentation rates. This prolonged 33,000 year period of reduced field strength and increased geomagnetic instability supports models that show frequent centennial-to-millennial-scale polarity changes in the presence of a strongly weakened dipole field.

1. Introduction

The last polarity reversal, from the reversed Matuyama Chron to the normal Brunhes Chron (M-B polarity reversal), is a critical stratigraphic marker for developing late-Cenozoic age models (Channell et al., 2010; Shackleton & Opdyke, 1973). Many age determinations for this M-B reversal come from astrochronologically tuned sediment records that also identify a strong reduction in the intensity of the magnetic field leading up to the reversal (Merrill & McFadden, 1994). However, due to low sedimentation rates, most sediment records may not resolve large and rapid directional changes associated with a weakened field strength prior to the M-B reversal (Channell et al., 2012; Coe & Glen, 2004; Roberts & Winklhofer, 2004). Volcanic sections dated by $^{40}Ar/^{39}Ar$ geochronology have the potential to capture such short-lived changes as they record ordered sequences of discrete snapshots of the Earth's magnetic field, but their occurrence is rare. At present only four volcanic records (Tahiti, Greenland, Hawaii, and Oregon, USA) are known that are detailed enough to demonstrate significant serial correlation of directional change across the transition in super-posed flows (Chauvin et al., 1990; Herrero-Bervera & Valet, 1999; Jarboe et al., 2011; Riisager et al., 2003). None of these records has a simple reversal path and the most detailed of them, a Miocene record with 75 transitional lava flows from the Steens Mountain, Oregon, also displays the most complex transitional behavior (Jarboe et al., 2011). The other three volcanic records are more discontinuous and have significantly fewer lava flows recording the transition. To resolve the detailed structure of temporal changes in field behavior during a transition requires a large number of well-dated lava flows in a single location or developing a stack that combines lava flows from multiple worldwide locations.

Applying these two geochronological approaches to the M-B reversal led to a fundamental disagreement about its age, with $^{40}Ar/^{39}Ar$ dating of lava flows suggesting it is as much as 24 kyr older than the ~773 ka age suggested by astrochronologically tuned sediment records (Channell, 2017a; Channell et al., 2010). In addition, recent work on the M-B boundary preserved in the Chiba section of Bose Peninsula, Japan has a coupled U/Pb and astrochronologic age of 770.2 ± 7.3 ka (Suganuma et al., 2015), which was further refined to 771.7 ka (Okada et al., 2017). Contrary to these ages, recent work using $^{40}Ar/^{39}Ar$ constrained ages have

suggested an older age for the onset of the Bruhnes chron. A tephra bracketed record of the M-B reversal from a Paleolake outcrop in central Italy provides an estimated sanidine age of 780.1 ± 0.8 ka and argues for a rapid reversal of the field (Niespolo et al., 2017; Sagnotti et al., 2014). In addition, sanidine $^{40}Ar/^{39}Ar$ ages for a series of Toba tuffs bracketing a reversal recorded in an ODP core, coupled with other archives may indicate an even older M-B age of ~784 ka (Mark et al., 2017). Accordingly, some have questioned the ^{40}K–^{40}Ar decay constant and the age of the Fish Canyon Tuff (FCT sanidine) geological standard used in the calculation of the $^{40}Ar/^{39}Ar$ ages (Channell et al., 2010; Singer, 2014). We note, however, that the same combination of methods provides concordant ages for other paleomagnetic events such as the Laschamp (Laj et al., 2014; Lascu et al., 2016) and Santa Rosa (Balbas et al., 2016) excursions, suggesting there may be another explanation for the apparent disagreement in the timing of the M-B reversal. Singer et al. (2005) proposed one such explanation whereby the older $^{40}Ar/^{39}Ar$ ages are in fact correct and, as such, constrain a transitional phase of unstable field behavior prior to the M-B reversal. Singer et al. (2005) noted that this transitional phase coincided with a period of global low-dipole intensity identified in sediment and ice-core paleointensity records that occurred ~15–20 kyr before the M-B reversal (so-called precursor event) (Channell et al., 2009; Hartl & Tauxe, 1996; Kent & Schneider, 1995; Raisbeck et al., 2006).

One of the key locations where transitional-phase lavas have been dated is in the Punaru'u Valley, Tahiti (Figure 1). Singer et al. (2005) reported $^{40}Ar/^{39}Ar$ ages on three such lavas: 804.0 ± 11.0 ka, 797.8 ± 9.4 ka,
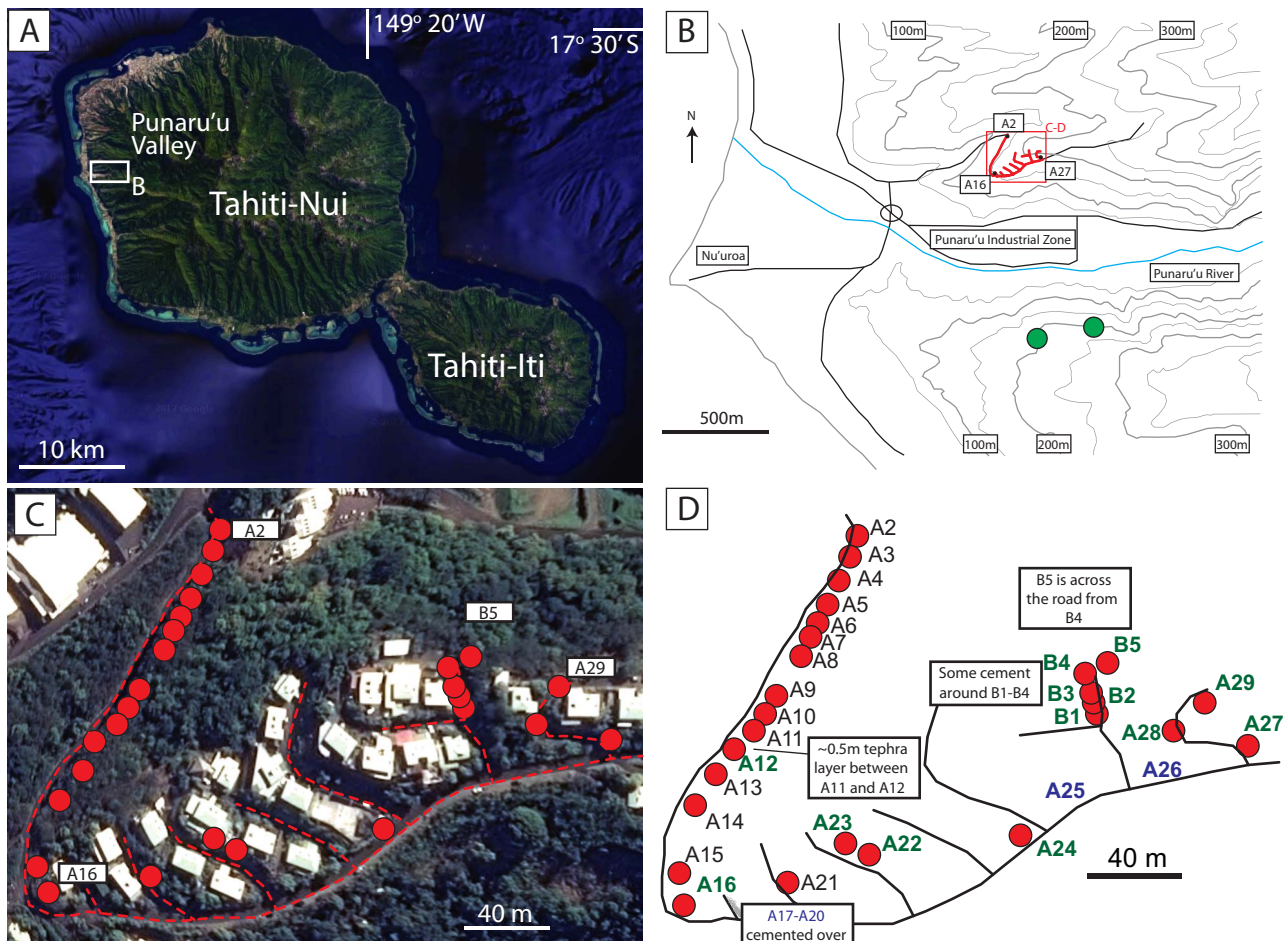

Figure 1. The location of samples used in this study. (a) A Google Earth® satellite image of Tahiti with the Punaru'u Valley shown (white box). (b) A contoured elevation map of the Punaru'u Valley adapted from Mochizuki et al. (2011). The location of the Matuyama-Brunhes transitional flows from Chauvin et al. (1990) flows are shown with green circles. The road is shown with black lines while the road outlined in plots (c)–(d) is colored red. The contour interval is 50 m (gray lines). (c) A satellite image of the housing development on the Northern side of the Punaru'u Valley. The locations of a few sampled flows are indicated with red circles. Outline of the road is shown with dash red line. (d) A simplified aerial reconstruction of the exposed lava flows sampled in this study (red circles). The black line indicates the location of roads outlines in plots (b)–(c). Individual flow exposures are labeled, with dated lava flows shown in green and nonsampled flows from Mochizuki et al. (2011) shown in blue.

Table 1
Summary of Stacked $^{40}Ar/^{39}Ar$ Age Results for Each Flow

		Age spectrum					Total fusion		Inverse isochron analyses		
Lava Flow	Material	Age ± 2σ (ka)	^{39}Ar %	K/Ca	MSWD	n steps	N total steps	N samples	Age ± 2σ (ka)	K/Ca	Age ± 2σ (ka)	$^{40}Ar/^{36}Ar$ intercept	MSWD
A12	Groundmass	**857.4 ± 3.5**	83	0.161	0.82	49	76	2	849.3 ± 4.4	0.462	854.4 ± 4.4	297.9 ± 2.14	0.73
A16	Groundmass	**816.1 ± 5.0**	62	0.062	0.89	22	70	2	809.4 ± 6.2	0.243	812.1 ± 10.1	297.8 ± 4.99	0.89
A22	Groundmass	**799.4 ± 4.3**	76	0.023	0.82	91	138	4	802.2 ± 5.4	0.204	802.2 ± 5.4	293.54 ± 2.76	0.81
A23	Groundmass	**800.9 ± 3.6**	53	0.206	0.88	41	98	3	811.1 ± 3.6	0.208	799.7 ± 9.3	296.95 ± 10	0.90
A24	Groundmass	**800.0 ± 3.6**	58	0.045	0.75	45	99	3	810.4 ± 4.1	0.222	799.6 ± 5.9	295.81 ± 2.91	0.77
A27	Groundmass	**795.1 ± 4.0**	80	0.044	0.52	85	139	4	798.9 ± 5.4	0.166	792.1 ± 5.6	297.34 ± 2.29	0.50
A28	Groundmass	**788.7 ± 3.1**	68	0.439	1.19	33	66	2	796.2 ± 3.2	0.386	781.7 ± 5.4	303.31 ± 5.11	1.19
A29	Groundmass	**805.1 ± 4.6**	82	0.075	0.66	59	96	3	825.3 ± 6.6	0.112	799.2 ± 6.3	301.34 ± 4.15	0.53
B1	Groundmass	**801.7 ± 2.9**	56	0.072	1.05	73	209	6	808.7 ± 3.4	0.216	798.4 ± 5.2	301.24 ± 7.05	1.02
B2	Groundmass	**793.7 ± 4.1**	51	0.218	1.74	58	177	5	816.2 ± 3.6	0.233	789 ± 5.7	301.66 ± 5.13	1.59
B3	Groundmass	**792.2 ± 4.8**	74	0.048	1.08	70	144	4	791.4 ± 6.7	0.138	788.9 ± 5.9	300.23 ± 3.82	1.01
B4	Groundmass	**781.3 ± 3.9**	90	0.071	0.96	113	139	4	782.7 ± 4.7	0.160	780.2 ± 5.1	296.02 ± 1.67	0.75
B5	Groundmass	**770.6 ± 5.9**	82	0.065	0.61	70	116	3	769.0 ± 7.2	0.155	772.5 ± 10.4	294.61 ± 4.22	0.61

Note. Each lava flow result is a stacked age based on incremental heating experiments from N independent samples taken 3–5 m apart. Here, n steps represents the number of heating steps used in the age calculation from N total steps analyzed in the experiment. ^{39}Ar (%) is the total amount of gas included in the weighted mean age. MSWD = mean square of weighted deviates.

and 804.0 ± 23.0 ka, recalibrated to the Kuiper et al. (2008) FCT sanidine standard age of 28.201 ± 0.046 Ma and the Min et al. (2000) decay constants. Mochizuki et al. (2011) reported $^{40}Ar/^{39}Ar$ ages on two additional transitional lavas: 770.0 ± 30.0 ka and 788.0 ± 37.0 ka (also recalibrated). As Singer (2014) noted, however, the large age uncertainties on these lavas (ranging from 9.4 to 37 ka at 2σ confidence levels) prevent their correlation to field behavior associated with the M-B precursor event or to the reversal itself.

Here we seek to build onto the work of Mochizuki et al. (2011) by providing new high-precision $^{40}Ar/^{39}Ar$ ages that have 2σ stacked uncertainties as low as 3.5 ka (Table 1) and by adding new paleomagnetic measurements from multiple lava flows on Tahiti that bracket the M-B polarity reversal. This work was undertaken to further constrain the age of the M-B reversal and test whether the event was a single rapid reversal (e.g., Sagnotti et al., 2014), two individual events (e.g., Channell et al., 2009; Hartl & Tauxe, 1996; Kent & Schneider, 1995; Raisbeck et al., 2006; Singer et al., 2005), or a prolonged period of instability (e.g., Valet et al., 2005). The new ages, in conjunction with paleomagnetic orientation and intensity data, indicate that geomagnetic instabilities persisted for at least ∼33 kyr prior to onset of the Bruhnes chron. A stochastic model is presented that helps to reconcile the age constraints from sedimentary archives with $^{40}Ar/^{39}Ar$ dated lava archives.

2. Geologic Setting

Chauvin et al. (1990) first documented the existence of several sequences of lava flows exposed within the Punaru'u Valley, Tahiti-Nui, that record anomalous paleomagnetic field orientations. Their K-Ar ages ranged from 0.62 to 1.19 Ma, potentially covering the M-B, Jaramillo, and Cobb Mountain reversals. Mochizuki et al. (2011) reoccupied the Punaru'u Valley and located the lava-flow sequence recording the M-B reversal within a new housing development on the northern side of the valley (Figure 1). The lava-flow sequence is discontinuous, with exposure being limited to various road cuts. The lava flows consist primarily of clinopyroxene and olivine phyric alkali basalts (including some ankaramites) that have erupted as flows ranging from 2 to 10 m in height. Distinct rubbly tops on each flow separate individual flows from each other with paleosol layers notably absent. Mochizuki et al. (2011) reported paleomagnetic field orientation and intensities for 34 flows that bracketed the M-B reversal and provided $^{40}Ar/^{39}Ar$ ages from six flows ranging in age from 866 ± 18 ka to 773 ± 30 ka. Mochizuki et al. (2011) noted that although these lava flows are similar in age (within the large uncertainty bounds) and in petrology to the samples studied by Chauvin et al. (1990) from the southern side of the valley (Figure 1), their directional records are significantly different so that individual flows cannot be directly correlated between the two sections.

3. Methods

3.1. Sampling

We reoccupied the field site of Mochizuki et al. (2011) and resampled Tahitian lava flows A2–A29 and B1–B5 for high-precision ^{40}Ar/^{39}Ar age determinations and paleomagnetic measurements (Figure 1). We collected six samples from each of the 27 flows for ^{40}Ar/^{39}Ar analyses and a minimal number (1–4) of oriented samples from each flow for paleomagnetic measurements. We sampled basalt with a holocrystalline groundmass from the freshest sections in the core of each massive flow, at least 1 m below their rubbly and weathered flow tops, following the same sampling rationale as applied in a study of a single 7 m thick basalt flow on Floreana Island in the Galapagos Archipelago (Balbas et al., 2016). Every effort was made to increase the horizontal spacing between samples to ensure that all samples are physically different (albeit only modestly) in terms of their petrology, geochemistry, physical volcanology, and alteration state. The average horizontal distance between samples was ∼3–4 m.

Where possible, we used the same sample identifications for flows as used by Mochizuki et al. (2011). The stratigraphic relationship and geologic context of the majority of these flows could not be resolved in the field due to obstruction by road cuts and general construction. Several homes cover the area and roads were constructed along the weaker, highly altered and fractured sections of basalt. Consequently, some road cuts, including flows A17–A20 from Mochizuki et al. (2011), are covered in cement to prevent rock fall. In addition, flow A1 was not sampled since it was not important to this study. Flows A25 and A26 were difficult to distinguish in the field and were not resampled. Accordingly, of the 34 flows analyzed in Mochizuki et al. (2011), we sampled 27 with the only exclusions being those listed above.

3.2. ^{40}Ar/^{39}Ar Geochronology

Samples were crushed and sieved to a grain size of 150–180 μm followed by removal of pyroxene and olivine by magnetic separation. Moderately magnetic groundmass separates were then acid leached following previously defined procedures (Balbas et al., 2016; Koppers et al., 2011). Samples were sonicated for four 1 h steps in 3N and 6N HCl and 1N and 3N HNO$_3$ followed by a 1 h sonication in ultrapure H$_2$O (Koppers et al., 2000, 2011). Samples were then oven dried overnight at 50°C. All samples were handpicked under a binocular microscope to avoid any alteration and the presence of adhering phenocryst fragments. Samples were loaded into aluminum packets and irradiated in the Oregon State University (OSU) TRIGA reactor for 6 h with Fish Canyon Tuff (FCT) sanidine flux monitors along with Alder Creek (AC-2) sanidine samples used as a secondary standard.

Samples were analyzed using the same protocol on a Thermo Scientific ARGUS VI multicollector mass spectrometer in the OSU Argon Geochronology Laboratory. Approximately 19 mg groundmass sample was loaded into copper trays and incrementally heated using a CO$_2$ laser for 33 steps with blanks run before, during, and after the analyses (a total of 14 blanks). Released gasses were cleaned for 6 min using four getters kept at, respectively, 400°C (ST101), 200°C (ST172), and room temperature (ST172, AP10). Samples were inlet into the ARGUS VI with ^{40}Ar, ^{39}Ar, ^{38}Ar, and ^{37}Ar measured simultaneously on four 10^{12} Ω Faraday cups, while the ^{36}Ar was measured on an ion-counting CuBe electron multiplier.

All ages were processed using ArArCALC v.2.7.0 (Koppers, 2002) with a Fish Canyon Tuff (FCT) sanidine as a flux monitor with an assigned age of 28.201 ± 0.046 Ma (2σ) (Kuiper et al., 2008) and the decay constant and equations of Min et al. (2000). All errors include corrections for baselines, blanks, irradiation, production ratios, radioactive decay, mass fractionation, and the multiplier/Faraday collector calibration on mass 36. Reproducibility of the secondary AC-2 sanidine standard is excellent, providing an age of 1,185.2 ± 3.8 ka; mean square of weighted deviates (MSWD): 6.62; N = 257/275, within error with the AC-2 age of 1,186.4 ± 1.2 ka from Jicha et al. (2016) measured on a Noblesse Nu-instruments multicollector mass spectrometer.

3.3. Paleomagnetic Methods

Paleomagnetic drill cores were taken from each of the lava flows sampled for ^{40}Ar/^{39}Ar dating solely to confirm that the flows are the same as those reported in Mochizuki et al. (2011). Typically, three cores were taken from each flow and were spaced as far apart as possible (1–5 m). Cores were oriented in the field with a Pomeroy stage with respect to magnetic north and corrected for the regional magnetic declination of 13°

east. Fifteen of the cores were also oriented by sun compass on the few occasions when this was possible, in order to assess and correct the deflection due to any local magnetic anomaly at the orienting stage.

One sample from each core was analyzed in the magnetically shielded room at the University of California, Santa Cruz paleomagnetic laboratory. Each sample was progressively demagnetized in a Sapphire SI-2 instrument using 19 alternating field (AF) steps ranging from 0 to 180 mT and measured after each step in a 2G cryogenic magnetometer. Best-fit lines, and in a few instances best-fit great circles, were determined by principal component analysis (Fisher, 1953; Kirschvink, 1980; McFadden & McElhinny, 1988). After removing a normal-polarity component at low AF steps, the majority of samples yielded a well-defined characteristic direction in principal-component analysis (supporting information Tables S14 and S15).

4. Results

4.1. ^{40}Ar/^{39}Ar Ages

Our new chronology is based on 57 high-precision ^{40}Ar/^{39}Ar ages on 13 basalt lava flows that span the M-B reversal and several tens of millennia before it. Our new ages range from 857.4 ± 3.5 ka to 770.6 ± 5.9 ka (all uncertainties in this study are 2σ internal errors; Table 1), covering the previously analyzed range by Mochizuki et al. (2011) (867 ± 18 ka to 770 ± 30 ka) but with significantly improved precision. To achieve these improved precisions, we carried out incremental heating experiments with an increased number of steps (33 versus 13–39 in Mochizuki et al., 2011; Singer et al., 2005) on carefully prepared crystalline groundmass samples, and we carried out between 2 and 6 repeat analyses on samples taken 3–4 m apart in the same lava flow. This approach allowed us to stack the resulting experiments (see Figure 2 for three representative stacks, supporting information Figures S1–S13 for all stacks), if the repeat analyses on different samples of the same lava flow provided concordant age results (at the 2σ confidence level). The stacked weighted mean and isochron ages are then calculated by combining these different experiments and by pooling the individual heating steps included into the age plateaus from each experiment. These stacks provide us with increased confidence that we can resolve the eruption ages independent of (small) differences in petrology (i.e., varying modal amounts of plagioclase, clinopyroxene, and interstitial glass in the groundmass), physical volcanology (i.e., vesicularity) and degrees of weathering.

Individual groundmass analyses (excluding B3-Ar-2, discussed below) resulted in age plateaus that are 37%–100% wide, include between 6 and 33 incremental heating steps, and have satisfactorily low MSWD values with an average of 0.8 (n = 45) and ranging from 0.1 to maximally 2.0. These individual plateaus have already increased precision, ranging from 3.5 to 13.1 ka, but after stacking precisions came further down to 2.9–5.9 ka. Most groundmass experiments show evidence for (modest) ^{39}Ar$_{(k)}$ recoil during the lowest temperature steps, when any remaining fine-grained alteration minerals are preferentially outgassing, but typically this is confined to the first ~20% of the argon gas released during incremental heating. It is important to note that our repeat experiments for singular lava flows also show differing amounts of low temperature ^{39}Ar$_{(k)}$ recoil, and in some cases, these result in markedly different K/Ca spectra (e.g., flows A23 and A29 in supporting information Figures S4 and S8). Despite these differences in sample character, our repeat analyses for single lava flows always produced concordant plateau ages at the 2σ confidence level. We take this as direct evidence that we successfully minimized recoil effects in the groundmass samples and can use between 40% and 80% of the gas released to determine the eruption ages for the Tahiti lava flows. The resulting stacked ^{40}Ar/^{39}Ar ages (Table 1) are in stratigraphic concordance (Figure 3) providing proof that the new ages are accurately representing the Punaru'u Valley eruption sequence. All but one groundmass sample contained atmospheric ^{40}Ar/^{36}Ar intercepts with corresponding inverse isochron ages that are concordant with the plateau ages. Only one sample (B3-Ar-2) was excluded from the mean flow age calculation for flow B3 (stacked age of 792.2 ± 4.8 ka) due to suspected excess Ar, which is evident in its significantly higher 901.5 ± 22.2 ka plateau age and 328.3 ± 12 nonatmospheric isochron intercept (supporting information Figure S11). See the supporting information Document for age plateaus, isochrons, and flow-by-flow descriptions.

4.2. Paleomagnetic Orientations

Mochizuki et al. (2011) performed hysteresis and thermomagnetic experiments to assess magnetic mineralogy and properties of the flows, yielding results like those of many suites of subaerial basalts. They indicate that remanence is carried by some combination of Ti-poor and Ti-rich titanomagnetite, sometimes partially
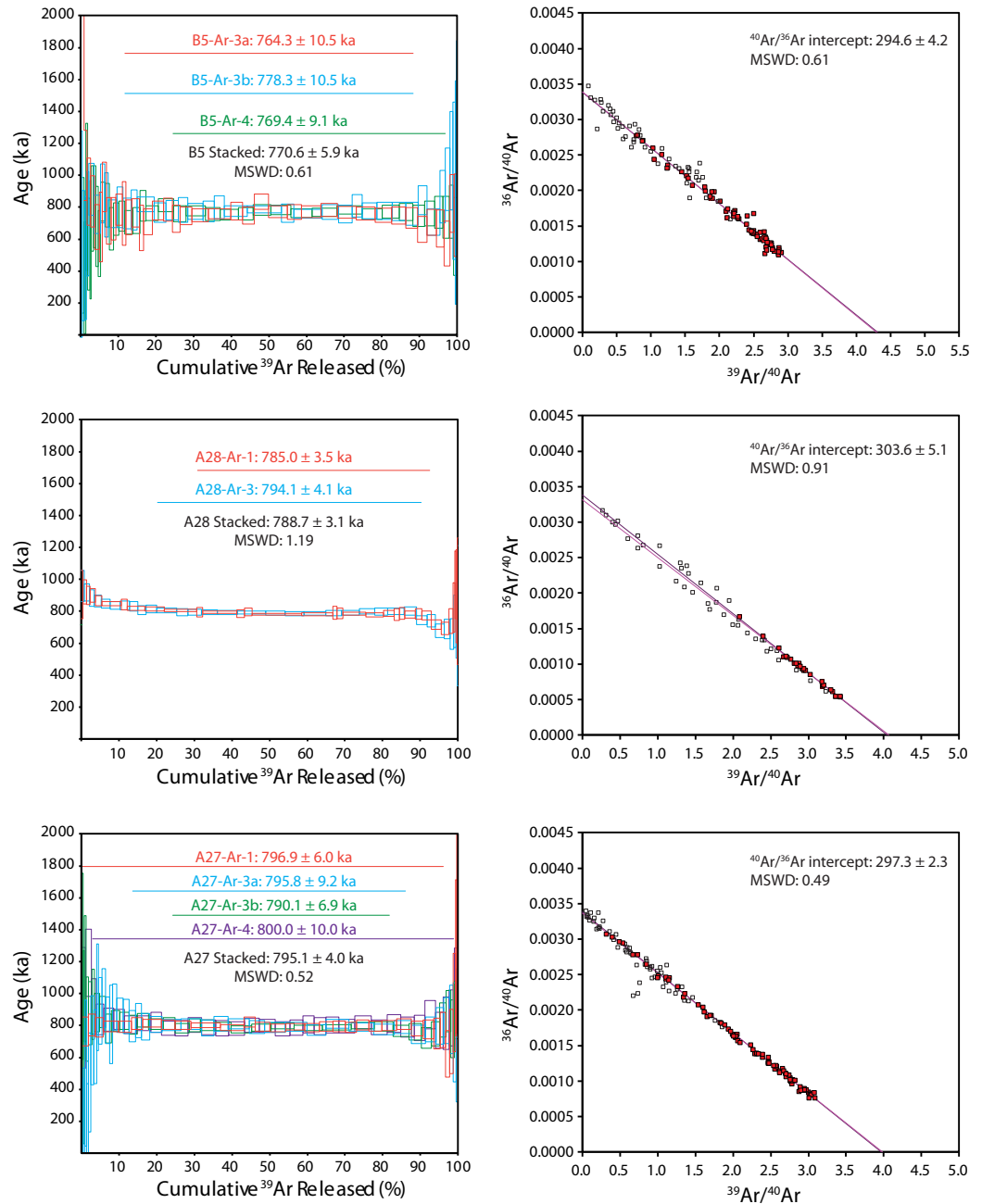
Figure 2. $^{40}Ar/^{39}Ar$ age results for the representative flows A27, A28, and B5. (left) Individual plateau results and the resulting plateau age and MSWD are shown. (right) Inverse isochron plots for the stacked age results. Red symbols represent values used to calculate the isochron (black line) while hollow symbols represent results that fell off of the plateau and were not used. An atmospheric reference line is shown (pink). All uncertainties are shown with 2σ confidence.

oxidized to titanomaghemite, and with pseudosingle domain hysteretic properties that usually signify a mixture of single-domain and multidomain grains. Such flows are typically good recorders of paleomagnetic direction.

We measured the paleomagnetic direction in 22 of the exposed basalt flows (supporting information Tables S14 and S15). Paleomagnetic directions obtained using sun-compass measurements of core azimuth (flows A16, A21, A27, A28, and A29) were preferred over magnetic measurements and are used in figures and models when available. Samples from flows A27 and A28 yielded sun-compass corrections to magnetic azimuths of 32° and 11°, respectively, whereas corrections for the remainder of cores were between 2° and 9°.
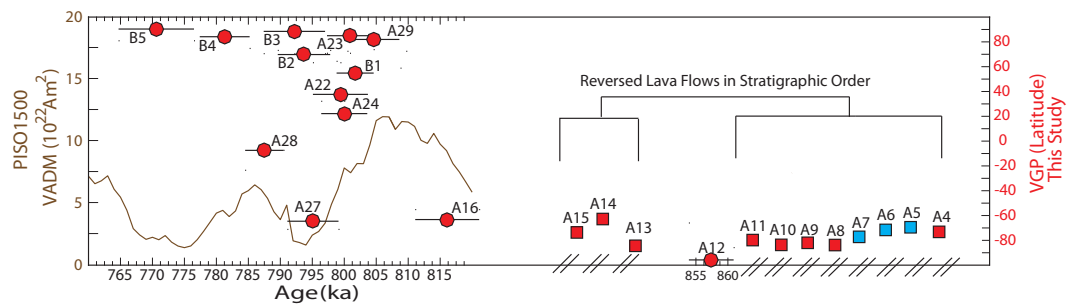
Figure 3. Paleomagnetic and age results from this study (red) and Mochizuki et al. (2011) (blue). Virtual axial dipole moment (VADM, brown line) of the PISO-1500 sediment core stack (Channell et al., 2009) and VGP for the Tahiti basalts plotted against age from well before to just after the Matuyama-Brunhes reversal. Hexagons represent age dated samples, while squares represent samples without age determinations. Hatched lines indicate the undated sample is positioned based on stratigraphic order. Undated flow A21 is not shown. All age determinations uncertainties are shown with 2σ confidence.

The natural remanent magnetism (NRM) for samples from flow A28 ranges up to 20 A m^{-1} (supporting information Table S15), large enough to produce local anomalies that could deflect the compass needle by 10° or more. However, the cores from flow A27 contained much lower NRM values around 1 A m^{-1}, indicating some other, unknown source for that large local deflection. In any case, the results for the great majority of the samples suggest that their magnetic and true geographic declinations probably differ by only 2°–10°, or too small a difference to affect our conclusions.

The sampled lava flows include normal, transitional, and reversed orientations. Most of the flows display concordant primary orientations throughout most of the alternating field steps. Some flows within the intermediate phase of the reversal show large viscous overprinting, which is probably enhanced by the weakness of the magnetic field during this period. The 13 oldest flows (A2–A16) all have reversed polarity; we dated two of these flows at 857.4 ± 3.5 ka (A12) and 816.1 ± 5.0 ka (A16) (Figure 3). The next 10 younger flows, in order of age range from 805.1 ± 4.6 ka (A29) to 781.3 ± 3.9 ka (B4) and have VGP latitudes that range consecutively from normal to transitional to normal to transitional to reversed to normal to transitional to normal (Figure 3). The youngest sample (B5) has a normal polarity that, according to its 770.6 ± 5.9 ka age, potentially formed after the main M-B reversal at 770–773 ka (Channell et al., 2010; Okada et al., 2017).

Our paleomagnetic data from the flows are in good agreement with the data from Mochizuki et al. (2011) at this location. The exceptions are flows A27 and B1 and, to a lesser extent, A22 and A28 (Figure 4). The discrepancy for all but A22, A24, A27, and B1 is no more than 29°, with an average of 11°. All of them are associated with paleointensity lows, as indicated by the exceptionally low NRM/ARM values (Mochizuki et al., 2011). Flows A27 and B1 differ by 159° and 129°, almost entirely in declination, but we are confident that we did not make a gross error in orienting these cores because their low-coercivity overprints are normal polarity, as they should be for a Brunhes-normal viscous remanence. Our measurement for B1 contains a large uncertainty ($\alpha 95 = 42°$) consistent with the relatively large secondary components previously observed from this flow (Mochizuki et al., 2011). A22 and A24, with angular discrepancies of 35° and 74°, differ significantly in both inclination and declination. Because our sample directions for both A22 and A24 cluster much better than those reported by Mochizuki et al. (2011), each having a precision parameter ~15 times larger, we suspect that the overprints on their samples could not be as completely removed as on ours. Thus, although the major conclusions of our study do not depend on which study's directions we choose, we use our values in the figures and models reported herein.

5. Discussion

5.1. Stratigraphy

Our additional field observations and high-precision ^{40}Ar/^{39}Ar ages better constrain the stratigraphic relationships first described by Mochizuki et al. (2011), with all ages associated with flows that are in direct contact being consistent with the law of superposition (A2 through A16 and B1 through B4; Figure 5). However,
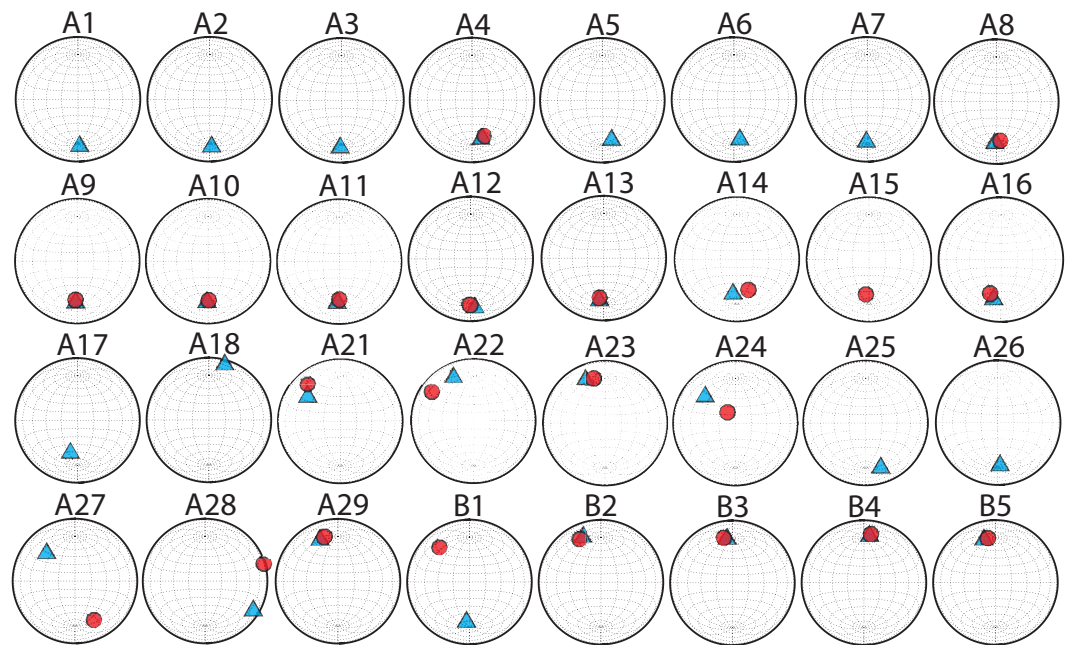
Figure 4. Mean virtual geomagnetic pole data for each individual flow from this study (red) and Mochizuki et al. (2011) (blue).

several flow contacts could not be identified given that the outcrops consist of several different road cuts whose stratigraphic relationships are obscured by the construction of residential homes (Figure 1) or that some flows sampled by Mochizuki et al. (2011) have since been cemented over. Moreover, our fieldwork and analyses indicate that higher elevation flows are not necessarily younger than lower elevation flows. For example, flow A29 is one of the oldest flows in the sequence (805.1 ± 4.6 ka), yet was sampled at the highest elevation on top of a steep cliff. This flow contains an age, inclination, and declination that lie within uncertainty of flow A23 (800.9 ± 3.6 ka), and thus potentially represent another outcrop of the same erupted lava. Flow A28 (788.7 ± 3.1 ka) is the second highest flow sampled. It only appears to crop out in one location and is petrologically distinct from all flows sampled (plagioclase phyric). These elevation and age relationships thus suggest a complicated depositional history with lava flows likely channeling toward and filling, local erosional features. Consequently, we use our new ages to establish paleomagnetic and stratigraphic ordering for flows without readily identifiable contacts (A24, A25, A26, A27, A28, and A29).
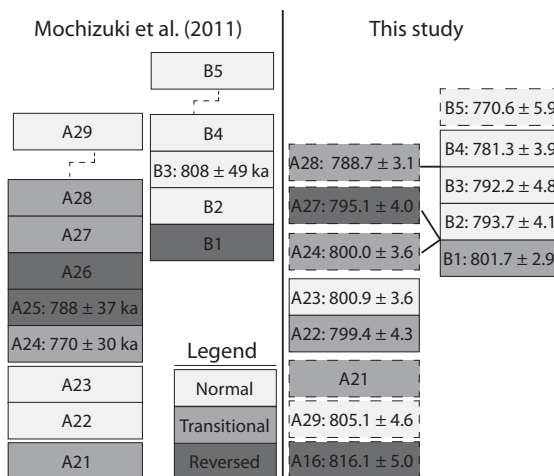

Figure 5. The stratigraphic order of sampled lava flows from Punaru'u Valley, Tahiti based on field relations (left; Mochizuki et al., 2011) and based on field relations and age determinations (right; this study). Boxes are shaded according to paleomagnetic orientations presented in Mochizuki et al. (2011) (left) or this study (right). Dashed outlines represent flows not observed to be in direct contact with other flows. Age determinations are shown with 2σ uncertainties (ka). Flows A25 and A26 were not resampled in this study and flow A21 does not have age determinations. Flows A2–A16 (not shown) are all reversed orientation and in stratigraphic order.

Figure 5 shows our reconstructed stratigraphy compared to the stratigraphy presented in Mochizuki et al. (2011). We did not resample flows A25 and A26. Our stratigraphy suggests that the most probable sequence of VGP latitudes prior to 773 ka, arranged from oldest to youngest, is R-N-T-N-T-R-N-T-N (Figure 5). This sequence differs from that suggested by Hoffman and Mochizuki (2012), who proposed that the precursor phase (780–800 ka) contains paleomagnetic orientations pointing toward Australia, which then flip closer to the final reversal, orientating toward NE North America. Instead, our sequence suggests that the orientation flips between nonaxial dipole locations frequently during the ~33 kyr prior to the Bruhnes chron. We note that simpler VGP sequences obtained by rearrangement of the flows that still satisfy our 2σ confidence limits are possible. For instance, moving A28 lower in the sequence so it lies between A27 and B2

simplifies the sequence to R-T-N-T-R-N, but the sequence still suggests several rapid changes in field orientation prior to the start of the Brunhes Chron.

5.2. The Instability Period Preceding the M-B Reversal

Understanding the length scales and patterns of the geomagnetic field prior to a reversal provides vital constraints for understanding the geodynamo. Before determining the length of the instability, an age for the final onset of the Bruhnes chron is required. There is significant debate over the age of the boundary with arguments for a ∼780–784 ka age (Cande & Kent, 1995; Mark et al., 2017; Niespolo et al., 2017; Sagnotti et al., 2014) or a ca. 772 ka age (Channell et al., 2010; Okada et al., 2017; Suganuma et al., 2010, 2015). Since lava flows provide only brief snapshots of instability we cannot directly provide an age for the reversal based on singular lava flow dating. The youngest flow with intermediate paleomagnetic orientation from the Tahiti sequence is A28 (788.7 ± 3.1 ka), which is proceeded by normally orientated flows. Thus, this may favor an older age for the onset of the M-B reversal. However, prior to the eruption of A28, there were multiple normally orientated flows with low field strength that indicate prolonged instability of the paleomagnetic field (Mochizuki et al., 2011). We favor the younger age for the M-B boundary (∼772 ka) as it is supported by different age determination methods from multiple disparate records, such as U/Pb (Okada et al., 2017; Suganuma et al., 2015), astrochronology (Channell et al., 2010), ice-core [10]Be records (Raisbeck et al., 2006; Suganuma et al., 2010), and one [40]Ar/[39]Ar age for a Hawaiian lava flow (Singer, 2014; Singer et al., 2005). In addition, the [40]Ar/[39]Ar age determinations supporting an older age for the M-B boundary were all analyzed using total fusion of single sanidine crystals (Mark et al., 2017; Sagnotti et al., 2014). However, it has recently been shown for the Bishop tuff that sanidine crystals may reside in relatively cool portions of its magma chamber for tens of thousands of years, allowing the ingrowth of excess radiogenic [40]Ar prior to eruption, making the sanidine ages slightly (but distinguishably) older than the eruption age (Andersen et al., 2017). The 780–784 ka older M-B ages are all constrained by similar sanidine analyses from equivalent silicic systems and, thus may have been influenced by magma chamber residence time issues as well, causing the resulting M-B boundary age estimates to be too old. More work is required from independent lava flow successions to lay this discussion topic to rest.
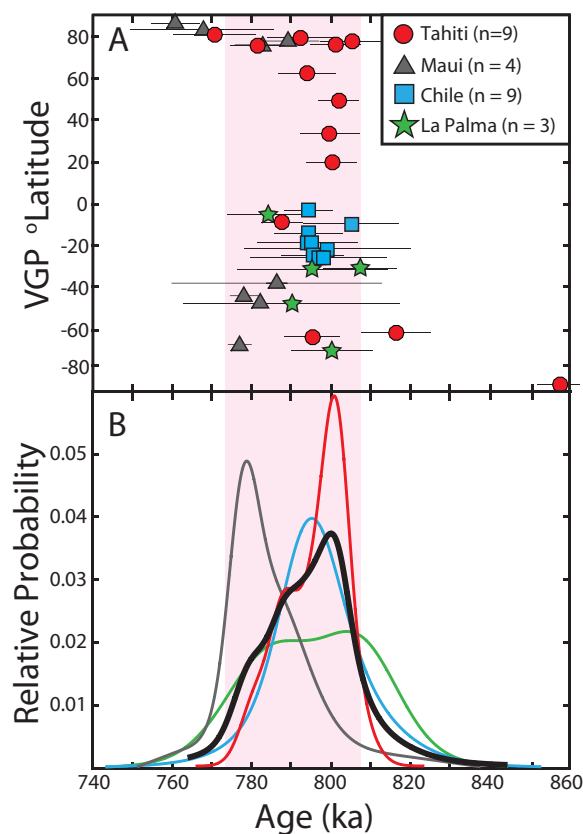
In order to determine the minimum length of instability prior to the Bruhnes Chron we compare our Tahitian constraints on magnetic field variability prior to the M-B reversal with similar evidence from other lava flow sequences dated by [40]Ar/[39]Ar (Brown et al., 2004; Singer et al., 2002) (Figure 6). We recalibrated all previously published [40]Ar/[39]Ar ages to the same [40]K decay constants and the FCTs standard age used for the Tahitian samples. Dated samples from the Maui site extend back to 785.1 ± 8.0 ka (Coe et al., 2004), while the La Palma and Chile samples largely occur between ∼790 and 810 ka, coincident with the precursor phase (Singer et al., 2005). VGP latitudes from these flows that are older than the M-B reversal range from reversed to normal, with a number of transitional directions clustered in the southern low latitudes. Here, we define field instability during the Matuyama Chron as any VGP between −45° and 90° latitude. Probability density functions (PDFs) of lava flows from Tahiti, Chile, and La Palma that meet this criterion suggest that much of this instability occurred between ∼795 and 805 ka; for Maui it is somewhat younger, being centered on ∼779 ka (Figure 6).

Some previous interpretations of this behavior from any given site suggested that its peak PDF age represented the M-B reversal, thus giving rise to some of the disagreement about the age of the reversal (Channell et al., 2010). Singer et al. (2005) proposed that the older transitional lavas from La Palma, Chile, and Tahiti record the onset of nondipolar field behavior that continued for ∼18 kyr until the M-B

Figure 6. Virtual geomagnetic pole (VGP) latitudes through time of all reported field sites that record the M-B reversal (Coe et al., 2004; Singer et al., 2005) with their corresponding probability density functions (PDF). The PDF curves incorporate only samples with latitudinal VGPs between −45° and 90°, which we interpret as indicating instability during the Matuyama chron. The black PDF curve is a combination of all site data with VGP's between −45° and 90°. All errors are displayed with 2σ uncertainty.

reversal recorded at Maui. Similar to Singer et al. (2005), we combine the data from all four sites into a composite record that, while still discontinuous, provides a more complete picture of global geomagnetic field behavior. The length of the instability defined by our sample set begins at 805.1 ± 4.6 Ma (A29) and, assuming a final reversal age of 771.7 ka (Okada et al., 2017), indicates that the field instability period persisted for ~33,000 yr. A PDF that includes all of the data supports the prolonged period of instability that extends from the M-B reversal at ~772 to ~805 ka (Figure 6), nearly twice as long as previously considered (Singer et al., 2005).

Additional ^{40}Ar/^{39}Ar dated records older than 805 ka are required to assess whether this unstable period might be longer. We also note that the frequency of the large polarity changes within this 33 kyr window suggests that large geomagnetic changes were occurring on a millennial and perhaps centennial timescale. This is particularly well demonstrated by our high-resolution dating of Tahitian flows, which identifies two large excursions between ~800 and 787 ka, while the Maui data show another large excursion between ~782 ka and the time of the actual M-B reversal (Figure 6).

5.3. Reconciling Lava Flow and Sediment Records

Well-dated, high-resolution sediment records from a range of latitudes show that VGPs often differ from stable-reversed directions during the 33 kyr interval prior to the M-B reversal, although their expression suggests a lower frequency in the polarity changes (Figure 7). We use a simple stochastic model to illustrate how a simulated geomagnetic signal would be recorded differently in volcanic and sedimentary archives. We assume that the Tahiti, Chile, La Palma, and Maui volcanic records capture random snapshots of directional variability occurring on century to millennial timescales (Constable & Johnson, 2005; Korte & Constable, 2006), whereas sediments record a more continuous signal that is smoothed as a result of sediment sampling method and the magnetization acquisition process (Egli & Zhao, 2015; Irving & Major, 1964; Lund & Keigwin, 1994; Roberts & Winklhofer, 2004; Verosub, 1977). For example, sediment smoothing is inherent to the sampling methods applied, whereby a 2 cm cubed discrete sample integrates 1 kyr of the magnetic record for sedimentation rates of 2 cm kyr^{-1} and u-channel samples integrate the paleomagnetic record based on the response function of the magnetometer, typically around 5–8 cm (Weeks et al., 1993) or 2.5–4 kyr for sedimentation rates of 2 cm kyr^{-1}. Additionally, measured sediment magnetizations are at least in part an integrated record of geomagnetic signal resulting from magnetic acquisition over a lock-in zone following deposition (Egli & Zhao, 2015; Mellström et al., 2015).

We created 1,000 artificial volcanic records at nominally 500 year intervals from 840 to 750 ka in a two-step process (Figure 8). In Step 1, we generated a reversed-to-normal M-B transition pattern by defining the Matuyama (reversed) and Brunhes (normal) chrons with the transition occurring at a given year randomly selected from a normal distribution based on the astrochronological age estimate of 773 ± 5 ka (Channell et al., 2010) (Figure 8a). While Channell et al. (2010) assign a 2σ error of 0.8 ka based on the standard deviation of five North Atlantic site estimates, this error does not consider uncertainty in the dating method itself (Martinson et al., 1987). We thus adopt a more conservative error estimate of ± 5 ka. At this step, directions are randomly assigned from a uniform distribution of reversed (–90° to –70° VGP latitude; 840 ka to transition) and normal (70° to 90° VGP latitude; transition to 750 ka) polarities.

In Step 2, we simulated the highly variable (secular) directional changes occurring during and preceding the M-B transition based on
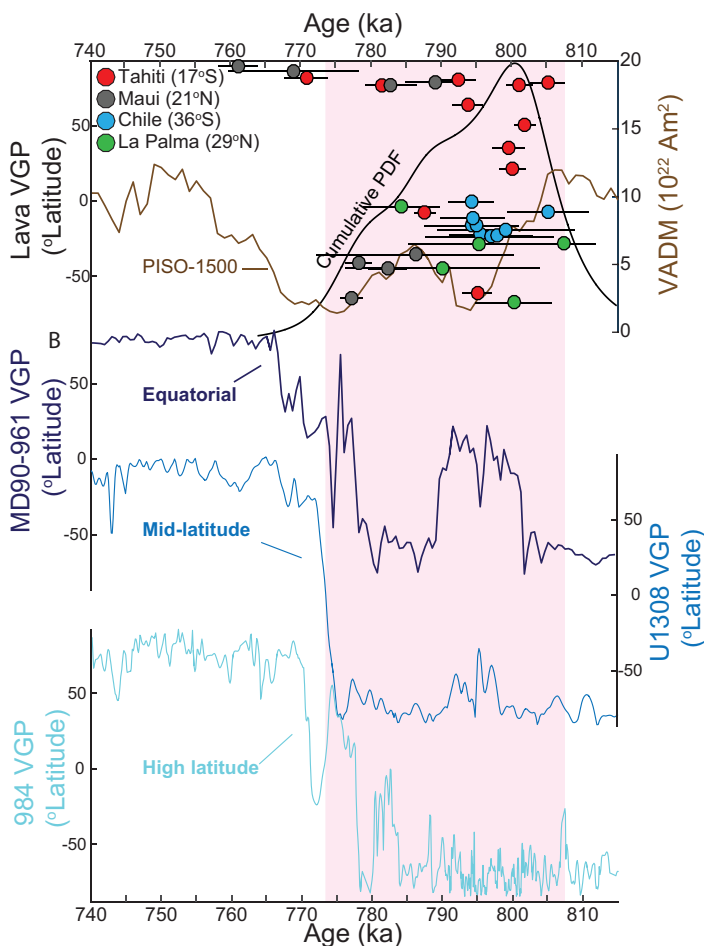

Figure 7. Latitudinal VGP variation of lava flow data compared to sediment core data from a range of latitudes. (top) All lava flow records from this time interval (circles) compared against PISO-1500 VADM stack (brown line). The black line represents the cumulative PDF curve for all lava flow data (Coe et al., 2004; Singer et al., 2005). (bottom) Astrochronologically tuned sediment cores ODP site 984 (Channell et al., 2002), with average sedimentation rate 11.5 cm kyr^{-1}; IODP site U1308 (Channell et al., 2008), with average sedimentation rate 7.3 cm kyr^{-1}); and MD90–961 (Channell et al., 2008), with average sedimentation rate 4.7 cm kyr^{-1}.
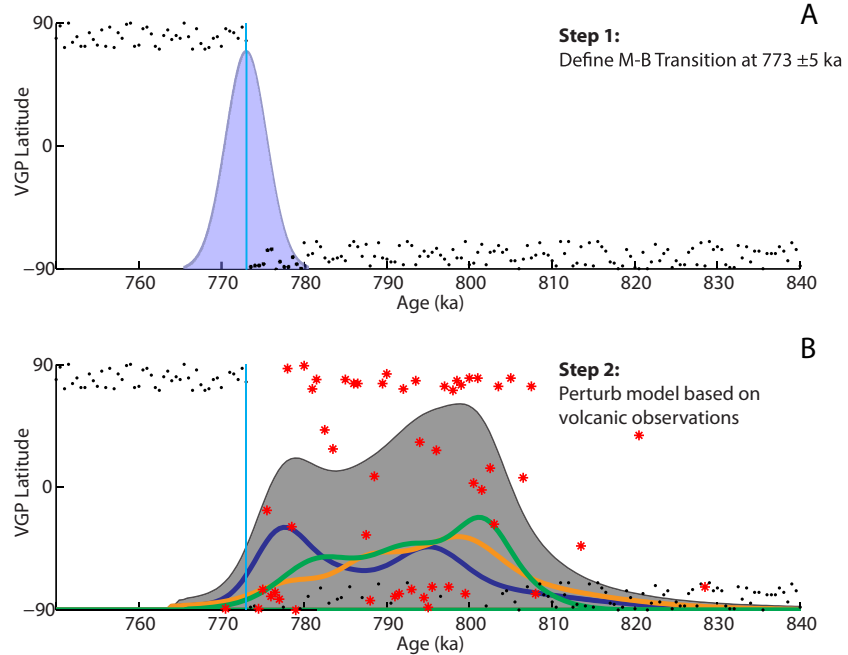
Figure 8. Illustrative description of one iteration of the simple model used in this discussion. (a) In the first step, reversed and normal directions (black dots) are assigned at 500 year time steps. The transition from reversed to normal occurs at randomly selected age from a normal distribution determined from astrochronological estimates, 773 ± 5 ka (2σ; purple shading and blue line) (Channell et al., 2010). (b) At each model time step, a random decision based on the summed volcanic record PDFs (gray shading) determines if the simple reversed-to-normal M-B transition pattern discussed above was either perturbed (red asterisks) or not (black dots). If the pattern was to be perturbed, a random selection based on the relative probability of having recorded an *observed* reversed, transitional or normal VGP at that time step (blue, orange, and green lines, respectively) then determined whether the *modeled* field was temporarily disturbed by having a reversed, transitional, or normal VGP.

the PDFs generated from the measured ages of Tahiti, Chile, La Palma, and Maui volcanic paleomagnetic records (Figure 6). At each model time step, the simple reversed-to-normal M-B transition pattern discussed above was either perturbed based on the summed volcanic record PDFs (gray shading in Figure 8b) or not, a so-called randomized decision point. If the pattern was to be perturbed, a random selection based on the relative probability of having recorded an observed reversed, transitional or normal VGP at that time step (blue, orange, and green lines, respectively, in Figure 8b), then determined whether the modeled field was temporarily disturbed by having a reversed, transitional, or normal VGP (red asterisks in Figure 8b and black dots in Figures 9–11). Perturbed directions were randomly assigned from three uniform directional distributions, using the latitudinal bins used to define the PDFs, that are either reversed (–90° to −45° VGP latitude), normal (45° to 90° VGP latitude), or transitional (–45° to 45° VGP latitude).

We then converted these artificial volcanic records to modeled sedimentary records using a simple Gaussian filter of variable width (by varying the Full Width Max Height (FWMH) from 1 to 20 kyr) to simulate the signal smoothing by sampling method and magnetic acquisition processes (red lines in Figures 9–11). While we apply this filter in time, we recognize the smoothing associated with magnetic acquisition processes occurs in depth. Assuming nominal 15 cm lock-in zones and steady sedimentation rates, these filter widths are likely most representative of sedimentation rates on the order of 10^{-1}–10^1 cm kyr^{-1}. The 95% confidence intervals for the model were generated from the 1,000 modeled sedimentary records (red shading Figures 9–11). For comparison, we plotted an example 95% confidence interval for an actual sedimentary record from the equatorial Indian Ocean based on its ± 5 ka age uncertainty (Valet et al., 2014), but not accounting for any uncertainty in the magnetic measurement (gray shading in Figures 9–11).

While this filtering approach does not account for possible offsets in time where the age of the magnetization may be younger than the age of the sediment, especially in low sedimentation rate locations (Channell & Guyodo, 2004; Ruddiman & Kent, 1990; Suganuma et al., 2010), it demonstrates how actual sedimentary
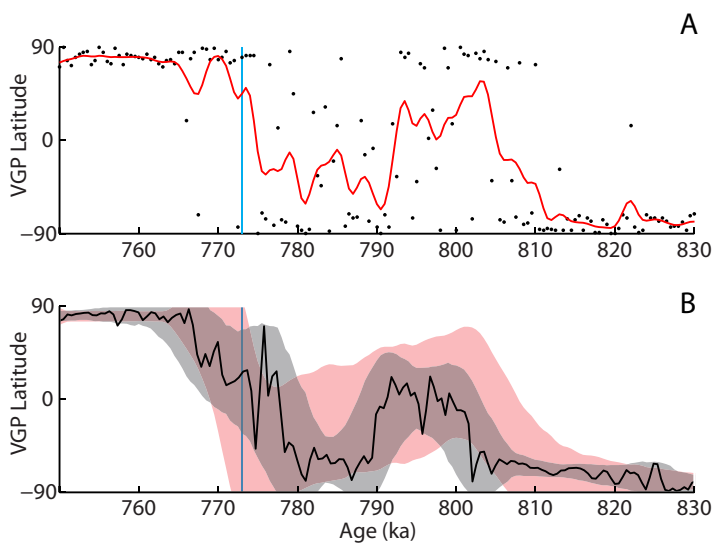
Figure 9. A simple model illustrates how volcanic and sedimentary records might record centennial to millennial scale variations of geomagnetic field directions differently. (a) One model run with an artificial volcanic record based on VGPs and $^{40}Ar/^{39}Ar$ ages from Tahiti, Chile, La Palma and Maui (black dots) and a modeled sedimentary record (red line) smoothed using a 2 kyr full width max height (FWMH) Gaussian filter (see text for details). (b) The 95% confidence interval of 1,000 modeled sedimentary records (red shading) compared with VGP latitude reconstruction from an Indian Ocean sediment core (black line) (Valet et al., 2014). Gray shading represents the 95% confidence interval for the actual sediment record based on its 5 ka age uncertainty (Valet et al., 2014). The vertical blue line at 773 ka marks a widely accepted age for the M-B transition from astrochronological estimates (Channell et al., 2010).

records may seemingly record subdued equatorial VGP latitudes for thousands of years while the volcanic records show extreme VGP directional short-term changes. The degree of smoothing in the sedimentary records increases when Gaussian filter widths are increased from 1 to 20 kyr (Figure 10). At the same time, the maximum VGP latitudes within our 95% confidence interval decrease significantly, from fully reversed/normal for Gaussian filter widths of less than about 7 kyr FWMH to almost completely transitional directions for wider filter widths.

Although these model runs show that the observed VGP latitude variations preceding the M-B transition in sediment records (equatorial and midlatitude examples in Figure 7) can be reproduced, the models cannot fully remove a positive upswing in VGP latitude around 795 ka (Figures 10 and 11) that is not observed in the high-latitude sedimentary record from ODP Site 984 (Channell et al., 2004). The exact reason for this discrepancy is unclear, but it could result from complex field morphologies at low-dipole field intensities (Brown & Korte, 2016; Brown et al., 2007; Clement, 2004; Valet & Plenier, 2008; Valet et al., 2012), complex sedimentation processes and/or magnetic acquisition, perhaps due to high-frequency variability in sedimentation rates (Channell, 1999). Assessing any of these options will require detailed study of globally distributed high-quality sedimentary records and a more complete understanding of the sediment magnetization acquisition process.

Additionally, it is interesting to note that when there is significant smoothing in our modeled sedimentary records (e.g., 20 kyr FWMH), the interpreted duration of the M-B transition is longer and the "midpoint" is older for the apparent reversal. However, this duration would likely seem more abrupt when sampling low-resolution (highly smoothed) sediments. Magnetic measurements are taken from 2 cm cubes, which can average upward of a thousand years. This illustrates the difficulty of making meaningful comparisons of globally distributed sedimentary records of variable and/or low resolution (Leonhardt & Fabian, 2007).

Our modeling shows that sedimentary sequences may record subdued equatorial VGP latitudes for thousands of years, while the volcanic records preserve extreme VGP directional short-term changes (Figures 8–11). With decreasing sedimentation rates, the maximum recorded sedimentary VGP latitudes also decrease significantly from steeper than 75° to transitional to almost absent. In addition, low-resolution sedimentary records may place the apparent M-B transition at older ages. Our results show that the general structure, timing and uncertainty of our stochastically modeled sedimentary VGP latitudes are consistent with high-quality sedimentary records (Figure 7). This simple model illustrates that given uncertainties related to chronologic, spatial/temporal coverage, and magnetic acquisition processes, the volcanic and sedimentary archives do record the same changes in the Earth's magnetic field, yet in different ways.

These results suggest that sedimentary and volcanic records of field variability prior to and during the M-B reversal are contemporary and related, supporting good agreement between the astrochronological and $^{40}Ar/^{39}Ar$ dating methods during the last million years. The onset of the prolonged period of directional instability identified from these records is coincident with the start of the precursor phase signified by a field intensity reduction that is well expressed in the PISO-1500 stack (Channell et al., 2009) (Figure 7). The majority of the transitional volcanic VGP latitudes recorded in lava flows from Tahiti, Maui, Chile, and La Palma are then coincident with a divergence from reversed field direction in some sediment records (Channell et al., 2008; Valet et al., 2014). This unstable field, coeval with the precursor phase of low-dipole intensity, suggests a period of heightened secular variation with large directional changes occurring on centennial to millennial timescales. These millennial or centennial variations in geomagnetic orientation are unlikely to be recorded in most sedimentary core records due to remanent magnetization acquisitions processes, nonuniform sedimentation rates and possible core disturbances (e.g., Channell, 2017b). Our results
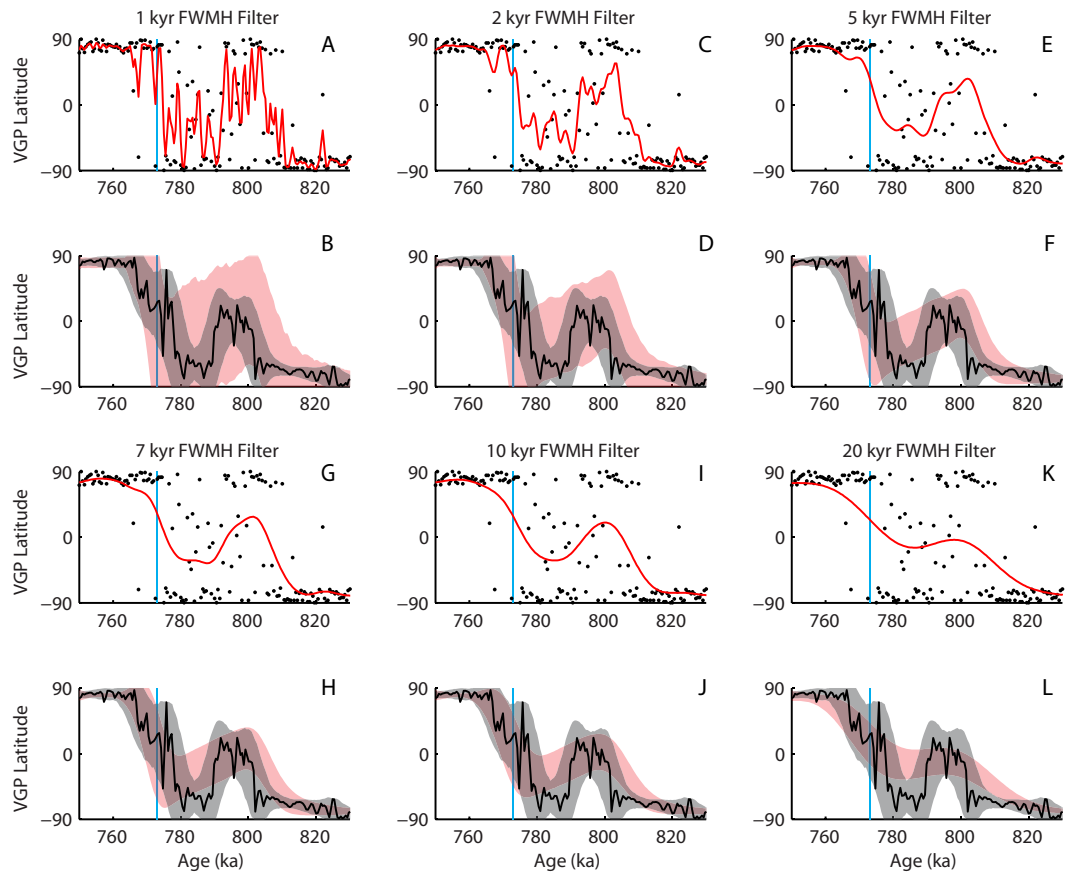
Figure 10. A simple model as described in Figure 8, except using variable Gaussian filter widths of (a, b) 1 kyr FWMH, (c, d) 2 kyr FWMH, (e, f) 5 kyr FWMH, (g, h) 7 kyr FWMH, (i, j) 10 kyr FWMH, and (k, l) 20 kyr FWMH.

are similar to descriptive models showing an increase in rapidly changing nondipole features (Brown & Korte, 2016; Brown et al., 2007; Valet & Plenier, 2008; Valet et al., 2012), when the field weakens. There are fewer observations of field instabilities from volcanic records (e.g., Maui) during a second phase of low-dipole intensity, which may suggest either a sampling bias or a relatively short-lived field instability immediately prior to the M-B reversal.
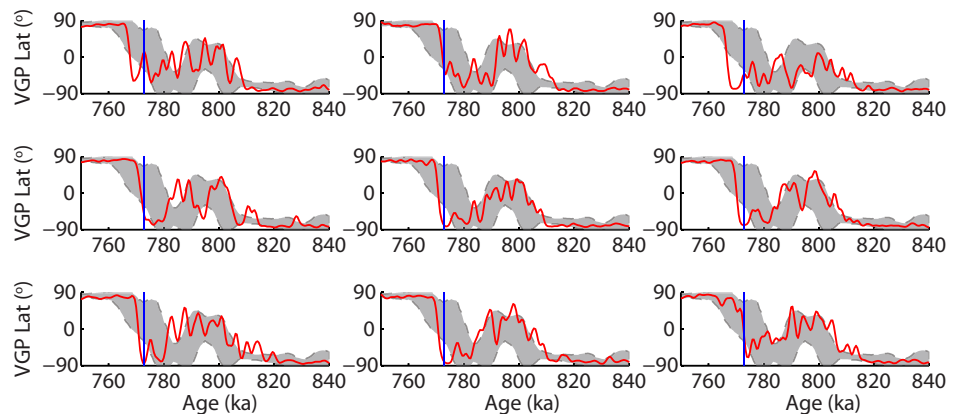

Figure 11. Nine random artificial sedimentary records created using a 2 kyr FWMH Gaussian filter (red lines) with the 95% confidence interval of an actual sedimentary record (gray shading; as in Figure 8). The vertical blue lines at 773 ka marks the age for the M-B transition from astrochronological estimates (Channell et al., 2010).

6. Conclusions

Our results provide important new insights into the short precursor history of a reversing field and the rapid—if not erratic—changing field dynamics during periods of low-dipole intensity. By reconciling volcanic and sedimentary records, we show that the instability prior to the onset of the normal Brunhes Chron lasted at least ∼33 kyr. The sedimentary and volcanic records of this well-studied event are in good agreement but can appear offset. This offset is likely due to natural smoothing of paleomagnetic directions recorded in sediment archives and the sporadic and limited nature of volcanic archives. It appears that large changes in VGP can occur on timescales less than those resolvable in such records.

The simple model provided here indicates that sedimentary records of paleomagnetic variability aren't appropriate to calibrate ^{40}Ar/^{39}Ar geochronologic standards. In addition, a single ^{40}Ar/^{39}Ar age determination on a transitionally orientated lava flow is not necessarily representative of the total timescale of the geomagnetic anomaly. We suggest that further combinations of multiple natural archives are vital for identifying more abrupt and short-lived paleomagnetic anomalies.

References

Andersen, N. L., Jicha, B. R., Singer, B. S., & Hildreth, W. (2017). Incremental heating of Bishop Tuff sanidine reveals preeruptive radiogenic Ar and rapid remobilization from cold storage. *Proceedings of the National Academy of Sciences of the United States of America*, *114*(47), 12407–12412.

Balbas, A., Koppers, A. A. P., Kent, D. V., Konrad, K., & Clark, P. U. (2016). Identification of the short-lived Santa Rosa geomagnetic excursion in lavas on Floreana Island (Galapagos) by ^{40}Ar/^{39}Ar geochronology. *Geology*, *44*(5), 359–362.

Brown, L. L., Singer, B. S., Pickens, J. C., & Jicha, B. R. (2004). Paleomagnetic directions and ^{40}Ar/^{39}Ar ages from the Tatara-San Pedro volcanic complex, Chilean Andes: Lava record of a Matuyama-Brunhes precursor? *Journal of Geophysical Research*, *109*, B12101. https://doi.org/10.1029/2004JB003007

Brown, M. C., Holme, R., & Bargery, A. (2007). Exploring the influence of the non-dipole field on magnetic records for field reversals and excursions. *Geophysical Journal International*, *168*(2), 541–550.

Brown, M. C., & Korte, M. (2016). A simple model for geomagnetic field excursions and inferences for palaeomagnetic observations. *Physics of the Earth and Planetary Interiors*, *254*, 1–11.

Cande, S. C., & Kent, D. V. (1995). Revised calibration of the geomagnetic polarity timescale for the Late Cretaceous and Cenozoic. *Journal of Geophysical Research*, *100*(B4), 6093–6095. https://doi.org/10.1029/94JB03098

Channell, J. E. T. (1999). Geomagnetic paleointensity and directional secular variation at Ocean Drilling Program (ODP) Site 984 (Bjorn Drift) since 500 ka: Comparisons with ODP Site 983 (Gardar Drift). *Journal of Geophysical Research*, *104*(B10), 22937–22951. https://doi.org/10.1029/1999JB900223

Channell, J. E. T. (2017a). Complexity in Matuyama-Brunhes polarity transitions from North Atlantic IODP/ODP deep-sea sites. *Earth and Planetary Science Letters*, *467*, 43–56.

Channell, J. E. T. (2017b). Magnetic excursions in the late Matuyama Chron (Olduvai to Matuyama-Brunhes boundary) from North Atlantic IODP sites. *Journal of Geophysical Research: Solid Earth*, *122*, 773–789. https://doi.org/10.1002/2016JB013616

Channell, J. E. T., Curtis, J. H., & Flower, B. P. (2004). The Matuyama-Brunhes boundary interval (500–900 ka) in North Atlantic drift sediments. *Geophysical Journal International*, *158*(2), 489–505.

Channell, J. E. T., & Guyodo, Y. (2004). The Matuyama Chronozone at ODP Site 982 (Rockall Bank): Evidence for decimeter-scale magnetization lock-in depths. In J. E. T. Channell et al. (Eds.), *Timescales of the paleomagnetic field, Geophysical Monograph Series* (Vol. 145, pp. 205–219). Washington, DC: American Geophysical Union.

Channell, J. E. T., Hodell, D., & Curtis, J. (2012). ODP Site 1063 (Bermuda Rise) revisited: Oxygen isotopes, excursions and paleointensity in the Brunhes Chron. *Geochemistry, Geophysics, Geosystems*, *13*, Q02001. https://doi.org/10.1029/2011GC003897

Channell, J. E. T., Hodell, D., Singer, B., & Xuan, C. (2010). Reconciling astrochronological and ^{40}Ar/^{39}Ar ages for the Matuyama-Brunhes boundary and late Matuyama Chron. *Geochemistry, Geophysics, Geosystems*, *11*, Q0AA12. https://doi.org/10.1029/2010GC003203

Channell, J. E. T., Hodell, D., Xuan, C., Mazaud, A., & Stoner, J. (2008). Age calibrated relative paleointensity for the last 1.5 Myr at IODP Site U1308 (North Atlantic). *Earth and Planetary Science Letters*, *274*(1), 59–71.

Channell, J. E. T., Mazaud, A., Sullivan, P., Turner, S., & Raymo, M. (2002). Geomagnetic excursions and paleointensities in the Matuyama Chron at Ocean Drilling Program sites 983 and 984 (Iceland Basin). *Journal of Geophysical Research*, *107*(B6), 2114. https://doi.org/10.1029/2001JB000491

Channell, J. E. T., Xuan, C., & Hodell, D. (2009). Stacking paleointensity and oxygen isotope data for the last 1.5 Myr (PISO-1500). *Earth and Planetary Science Letters*, *283*(1), 14–23.

Chauvin, A., Roperch, P., & Duncan, R. A. (1990). Records of geomagnetic reversals from volcanic islands of French Polynesia: 2. Paleomagnetic study of a flow sequence (1.2–0.6 Ma) from the island of Tahiti and discussion of reversal models. *Journal of Geophysical Research*, *95*(B3), 2727–2752. https://doi.org/10.1029/JB095iB03p02727

Clement, B. M. (2004). Dependence of the duration of geomagnetic polarity reversals on site latitude. *Nature*, *428*(6983), 637–640.

Coe, R. S., & Glen, J. M. G. (2004). The complexity of reversals. In J. E. T. Channell et al. (Eds.), *Timescales of the paleomagnetic field, Geophysical Monograph Series* (Vol. 145, pp. 221–232). Washington, DC: American Geophysical Union.

Coe, R. S., Singer, B. S., Pringle, M. S., & Zhao, X. (2004). Matuyama-Brunhes reversal and Kamikatsura event on Maui: Paleomagnetic directions, ^{40}Ar/^{39}Ar ages and implications. *Earth and Planetary Science Letters*, *222*(2), 667–684.

Constable, C., & Johnson, C. (2005). A paleomagnetic power spectrum. *Physics of the Earth and Planetary Interiors*, *153*(1), 61–73.

Egli, R., & Zhao, X. (2015). Natural remanent magnetization acquisition in bioturbated sediment: general theory and implications for relative paleointensity reconstructions. *Geochemistry, Geophysics, Geosystems*, *16*, 995–1016. https://doi.org/10.1002/2014GC005672

Fisher, R. (1953). Dispersion on a sphere. *Proceedings of the Royal Society of London. Series A, Mathematical and Physical Sciences*, *217*(1130), 295–305.

Google Maps® (2017). Tahiti-Nui, French Polynesia. Retrieved from https://www.google.com/maps/dir//-17.6506695,-149.4649036/@-17.6457311,-149.5175946,76991m/data=!3m1!1e3

Hartl, P., & Tauxe, L. (1996). A precursor to the Matuyama/Brunhes transition-field instability as recorded in pelagic sediments. *Earth and Planetary Science Letters*, *138*(1), 121–135.

Herrero-Bervera, E., & Valet, J.-P. (1999). Paleosecular variation during sequential geomagnetic reversals from Hawaii. *Earth and Planetary Science Letters*, *171*(1), 139–148.

Hoffman, K. A., & Mochizuki, N. (2012). Evidence of a partitioned dynamo reversal process from paleomagnetic recordings in Tahitian lavas. *Geophysical Research Letters*, *39*, L06303. https://doi.org/10.1029/2011GL050830

Irving, E., & Major, A. (1964). Post-depositional detrital remanent magnetization in a synthetic sediment. *Sedimentology*, *3*(2), 135–143.

Jarboe, N. A., Coe, R. S., & Glen, J. M. G. (2011). Evidence from lava flows for complex polarity transitions: the new composite Steens Mountain reversal record. *Geophysical Journal International*, *186*(2), 580–602.

Jicha, B. R., Singer, B. S., & Sobol, P. (2016). Re-evaluation of the ages of ^{40}Ar/^{39}Ar sanidine standards and supereruptions in the western US using a Noblesse multi-collector mass spectrometer. *Chemical Geology*, *431*, 54–66.

Kent, D. V., & Schneider, D. A. (1995). Correlation of paleointensity variation records in the Brunhes/Matuyama polarity transition interval. *Earth and Planetary Science Letters*, *129*(1), 135–144.

Kirschvink, J. L. (1980). The least-squares line and plane and the analysis of palaeomagnetic data. *Geophysical Journal International*, *62*(3), 699–718.

Koppers, A. A. (2002). ArArCALC—Software for ^{40}Ar/^{39}Ar age calculations. *Computers & Geosciences*, *28*(5), 605–619.

Koppers, A. A., Gowen, M. D., Colwell, L. E., Gee, J. S., Lonsdale, P. F., Mahoney, J. J., et al. (2011). New ^{40}Ar/^{39}Ar age progression for the Louisville hot spot trail and implications for inter-hot spot motion. *Geochemistry, Geophysics, Geosystems*, *12*, Q0AM02. https://doi.org/10.1029/2011GC003804

Koppers, A. A., Staudigel, H., & Wijbrans, J. R. (2000). Dating crystalline groundmass separates of altered Cretaceous seamount basalts by the ^{40}Ar/^{39}Ar incremental heating technique. *Chemical Geology*, *166*(1), 139–158.

Korte, M., & Constable, C. G. (2006). Centennial to millennial geomagnetic secular variation. *Geophysical Journal International*, *167*(1), 43–52.

Kuiper, K., Deino, A., Hilgen, F., Krijgsman, W., Renne, P., & Wijbrans, J. (2008). Synchronizing rock clocks of Earth history. *Science*, *320*(5875), 500–504.

Laj, C., Guillou, H., & Kissel, C. (2014). Dynamics of the earth magnetic field in the 10–75 kyr period comprising the Laschamp and Mono Lake excursions: New results from the French Chaîne des Puys in a global perspective. *Earth and Planetary Science Letters*, *387*, 184–197.

Lascu, I., Feinberg, J. M., Dorale, J. A., Cheng, H., & Edwards, R. L. (2016). Age of the Laschamp excursion determined by U-Th dating of a speleothem geomagnetic record from North America. *Geology*, *44*(2), 139–142.

Leonhardt, R., & Fabian, K. (2007). Paleomagnetic reconstruction of the global geomagnetic field evolution during the Matuyama/Brunhes transition: Iterative Bayesian inversion and independent verification. *Earth and Planetary Science Letters*, *253*(1), 172–195.

Lund, S. P., & Keigwin, L. (1994). Measurement of the degree of smoothing in sediment paleomagnetic secular variation records: An example from late Quaternary deep-sea sediments of the Bermuda Rise, western North Atlantic Ocean. *Earth and Planetary Science Letters*, *122*(3–4), 317–330.

Mark, D. F., Renne, P. R., Dymock, R. C., Smith, V. C., Simon, J. I., Morgan, L. E., et al. (2017). High-precision ^{40}Ar/^{39}Ar dating of Pleistocene tuffs and temporal anchoring of the Matuyama-Brunhes boundary. *Quaternary Geochronology*, *39*, 1–23.

Martinson, D. G., Pisias, N. G., Hays, J. D., Imbrie, J., Moore, T. C., & Shackleton, N. J. (1987). Age dating and the orbital theory of the ice ages: Development of a high-resolution 0 to 300,000-year chronostratigraphy 1. *Quaternary Research*, *27*(1), 1–29.

McFadden, P. L., & McElhinny, M. W. (1988). The combined analysis of remagnetization circles and direct observations in palaeomagnetism. *Earth and Planetary Science Letters*, *87*(1–2), 161–172.

Mellström, A., Nilsson, A., Stanton, T., Muscheler, R., Snowball, I., & Suttie, N. (2015). Post-depositional remanent magnetization lock-in depth in precisely dated varved sediments assessed by archaeomagnetic field models. *Earth and Planetary Science Letters*, *410*, 186–196.

Merrill, R. T., & Mcfadden, P. L. (1994). Geomagnetic-field stability—Reversal events and excursions. *Earth and Planetary Science Letters*, *121*(1–2), 57–69.

Min, K., Mundil, R., Renne, P. R., & Ludwig, K. R. (2000). A test for systematic errors in ^{40}Ar/^{39}Ar geochronology through comparison with U/Pb analysis of a 1.1-Ga rhyolite. *Geochimica et Cosmochimica Acta*, *64*(1), 73–98.

Mochizuki, N., Oda, H., Ishizuka, O., Yamazaki, T., & Tsunakawa, H. (2011). Paleointensity variation across the Matuyama-Brunhes polarity transition: Observations from lavas at Punaruu Valley, Tahiti. *Journal of Geophysical Research*, *116*, B06103. https://doi.org/10.1029/2010JB008093

Niespolo, E. M., Rutte, D., Deino, A. L., & Renne, P. R. (2017). Intercalibration and age of the Alder Creek sanidine ^{40}Ar/^{39}Ar standard. *Quaternary Geochronology*, *39*, 205–213.

Okada, M., Suganuma, Y., Haneda, Y., & Kazaoka, O. (2017). Paleomagnetic direction and paleointensity variations during the Matuyama-Brunhes polarity transition from a marine succession in the Chiba composite section of the Boso Peninsula, central Japan. *Earth, Planets and Space*, *69*(1), 45.

Raisbeck, G., Yiou, F., Cattani, O., & Jouzel, J. (2006). ^{10}Be evidence for the Matuyama-Brunhes geomagnetic reversal in the EPICA Dome C ice core. *Nature*, *444*(7115), 82–84.

Riisager, J., Riisager, P., & Pedersen, A. K. (2003). The C27n–C26r geomagnetic polarity reversal recorded in the west Greenland flood basalt province: How complex is the transitional field? *Journal of Geophysical Research*, *108*(B3), 2155. https://doi.org/10.1029/2002JB002124

Roberts, A. P., & Winklhofer, M. (2004). Why are geomagnetic excursions not always recorded in sediments? Constraints from post-depositional remanent magnetization lock-in modelling. *Earth and Planetary Science Letters*, *227*(3), 345–359.

Ruddiman, W. F., & Kent, D. V. (1990). Depth of post-depositional remanence acquisition in deep-sea sediments: A case study of the Brunhes-Matuyama reversal and oxygen isotopic stage 19.1. *Earth and Planetary Science Letters*, *99*(1), 1–13.

Sagnotti, L., Scardia, G., Giaccio, B., Liddicoat, J. C., Nomade, S., Renne, P. R., et al. (2014). Extremely rapid directional change during Matuyama-Brunhes geomagnetic polarity reversal. *Geophysical Journal International*, *199*(2), 1110–1124.

Shackleton, N. J., & Opdyke, N. D. (1973). Oxygen isotope and palaeomagnetic stratigraphy of equatorial Pacific core V28–238: Oxygen isotope temperatures and ice volumes on a 10^5 year and 10^6 year scale. *Quaternary Research*, *3*(1), 39–55.

Singer, B. S. (2014). A quaternary geomagnetic instability time scale. *Quaternary Geochronology*, *21*, 29–52.

Singer, B. S., Hoffman, K. A., Coe, R. S., Brown, L. L., Jicha, B. R., Pringle, M. S., et al. (2005). Structural and temporal requirements for geomagnetic field reversal deduced from lava flows. *Nature*, *434*(7033), 633–636.

Singer, B. S., Relle, M., Hoffman, K., Battle, A., Laj, C., Guillou, H., et al. (2002). Ar/Ar ages from transitionally magnetized lavas on La Palma, Canary Islands, and the geomagnetic instability timescale. *Journal of Geophysical Research*, *107*(B11), 2307. https://doi.org/10.1029/2001JB001613

Suganuma, Y., Okada, M., Horie, K., Kaiden, H., Takehara, M., Senda, R., et al. (2015). Age of Matuyama-Brunhes boundary constrained by U-Pb zircon dating of a widespread tephra. *Geology*, *43*(6), 491–494.

Suganuma, Y., Yokoyama, Y., Yamazaki, T., Kawamura, K., Horng, C.-S., & Matsuzaki, H. (2010). [10]Be evidence for delayed acquisition of remanent magnetization in marine sediments: Implication for a new age for the Matuyama-Brunhes boundary. *Earth and Planetary Science Letters*, *296*(3), 443–450.

Valet, J.-P., Bassinot, F., Bouilloux, A., Bourlès, D., Nomade, S., Guillou, V., et al. (2014). Geomagnetic, cosmogenic and climatic changes across the last geomagnetic reversal from Equatorial Indian Ocean sediments. *Earth and Planetary Science Letters*, *397*, 67–79.

Valet, J.-P., Fournier, A., Courtillot, V., & Herrero-Bervera, E. (2012). Dynamical similarity of geomagnetic field reversals. *Nature*, *490*(7418), 89–93.

Valet, J.-P., Meynadier, L., & Guyodo, Y. (2005). Geomagnetic dipole strength and reversal rate over the past two million years. *Nature*, *435*(7043), 802–805.

Valet, J.-P., & Plenier, G. (2008). Simulations of a time-varying non-dipole field during geomagnetic reversals and excursions. *Physics of the Earth and Planetary Interiors*, *169*(1), 178–193.

Verosub, K. L. (1977). Depositional and postdepositional processes in the magnetization of sediments. *Reviews of Geophysics*, *15*(2), 129–143. https://doi.org/10.1029/RG015i002p00129

Weeks, R., Laj, C., Endignoux, L., Fuller, M., Roberts, A., Manganne, R., et al. (1993). Improvements in long-core measurement techniques: applications in palaeomagnetism and palaeoceanography. *Geophysical Journal International*, *114*(3), 651–662.